# Resonance Raman Spectroscopy Reveals the Origin of an Intermediate Wavelength Form in Photoactive Yellow Protein†

Samir F. El-Mashtoly,‡ Masashi Unno,*,‡ Masato Kumauchi,§ Norio Hamada,|| Kimiyo Fujiwara,§ Jun Sasaki,§ Yasushi Imamoto,⊥ Mikio Kataoka,⊥ Fumio Tokunaga,§ and Seigo Yamauchi*,‡

*Institute of Multidisciplinary Research for Advanced Materials, Tohoku University, Sendai 980-8577, Japan, Department of Earth and Space Science, Graduate School of Science, Osaka University, Toyonaka, Osaka 560-0043, Japan, JST, CREST, Osaka University, Suita, Osaka 565-0871, Japan, and Graduate School of Materials Science, Nara Institute of Science and Technology, Ikoma, Nara 630-0192, Japan*

*Received September 11, 2003; Revised Manuscript Received December 10, 2003*

ABSTRACT: Photoactive yellow protein (PYP) is a bacterial blue light receptor containing a 4-hydroxycinnamyl chromophore, and its absorption maximum is 446 nm. In a dark state, the hydroxyl group of the chromophore is deprotonated and forms hydrogen bonds with Tyr42 and Glu46. Either removal of a hydrogen bond with Tyr42 or addition of chaotropes such as thiocyanate produces a blue-shifted species called an intermediate wavelength form, in which absorption maximum ranges from 355 to 400 nm. To examine the structural origin of the intermediate wavelength form, we have performed resonance Raman investigations of wild-type PYP and some mutants (Tyr42 → Ala, Tyr42 → Phe, Glu46 → Gln, and Thr50 → Val) in the presence or absence of potassium thiocyanate. These studies show that the chromophore of the intermediate wavelength form is protonated, implying an increase in a p$K_a$ of the chromophore. Hence, the removal of the hydrogen bond between Tyr42 and chromophore or partial protein denaturation in the presence of thiocyanate results in a spectral blue-shift. Quantum chemical calculations based on density functional theory further support the idea that the p$K_a$ of the chromophore is increased by removing a hydrogen bond or by increasing the dielectric constant in the vicinity of the chromophore.

The photoactive yellow protein (PYP)[1] from phototrophic bacterium *Halorhodospira halophila* is a small water-soluble photoreceptor protein (*1*), and it has been an attractive model for studying protein structures and dynamics. Recently, PYP gained further attention as the structural prototype for the PAS and LOV domains of a large class of receptor proteins (*2*). This protein has the 4-hydroxycinnamyl chromophore, which is covalently linked to Cys69 through a thiolester bond (*3*, *4*). In a dark state ($PYP_{dark}$), the chromophore is stabilized in the trans configuration as a phenolate anion (*5*−*8*). The phenolate oxygen O1 of the chromophore hydrogen bonds with the hydroxyl group of Tyr42 and the protonated carboxyl group of Glu46. The side chain oxygen of Thr50 hydrogen bonds with the OH group of Tyr42 (Figure 1). Photoexcitation of PYP triggers a photocycle that involves at least two intermediate states, denoted $PYP_L$ (also called $I_1$ or pR) and $PYP_M$ (also called $I_2$ or pB) (*3*, *9*−*14*). A long-lived blue-shifted $PYP_M$ intermediate is the putative signaling state of this photoreceptor protein.

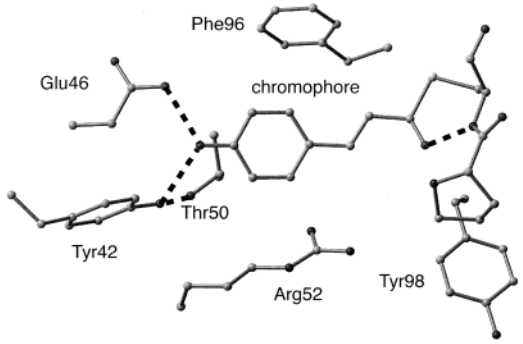


FIGURE 1: Active-site structure of wild-type PYP in the dark state (*5*). Dotted lines indicate hydrogen bonds.

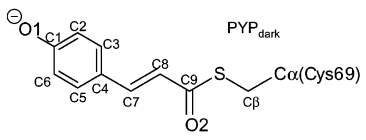


*H. halophila* displays negative phototaxis to blue light, and PYP has been proposed to function as the photosensor in this response (*15*). An absorption maximum of wild-type (WT) PYP is 446 nm, which results in its bright yellow color (*1*). However, a replacement of amino acid residues near the chromophore or changing solution conditions leads to a formation of different species in which the absorption

† This work was supported by grants from the Association for the Progress of New Chemistry to M.U. and by Grants-in-Aids 10780399 (M.U.) and 13354008 (S.Y.) from the Ministry of Education, Culture, Science, Sports, and Technology.

* To whom correspondence should be addressed. Tel: +81-22-217-5618. Fax: +81-22-217-5616. E-mail: (M.U.) unno@tagen.tohoku.ac.jp or (S.Y.) yamauchi@tagen.tohoku.ac.jp.

‡ Tohoku University.

§ Osaka University.

|| JST.

⊥ Nara Institute of Science and Technology.

[1] Abbreviations: DFT, density functional theory; FT, Fourier transform; HCMT, 4-hydroxycinnamyl methyl thiol ester; LOV, light, oxygen, or voltage; PAS, Per-ARNT-Sim; PYP, photoactive yellow protein; WT, wild-type.

10.1021/bi035638c CCC: $27.50 
Published on Web 01/30/2004

maximum is shifted remarkably. These species are recently classified into four groups (*16*): a neutral form (446−476 nm), an acidic form (350−355 nm), an alkaline form (430−440 nm), and an intermediate wavelength form (355−400 nm). As mentioned previously, the phenolic O1 in the neutral form is deprotonated (*6*−*8*), whereas the chromophore in the acidic form[2] is protonated (*17*) as a secondary result of acid denaturation (*16*). Protonation of the chromophore accounts for a large blue shift of the absorption maximum from 446−476 to 350−355 nm. The chromophore in the alkaline form is deprotonated like a neutral form, but the carboxylic group of Glu46 is suggested to be ionized (*16*).

In contrast to these forms, the origin of the intermediate wavelength form has not yet been clarified. This form was first found as a shoulder at 393 nm on the 458 nm peak in the absorption spectrum of Tyr42 → Phe mutant PYP (*19*). Subsequent studies showed an existence of similar intermediate wavelength forms when Tyr42 is replaced with Ala, Phe, or Trp (*10*, *16*). More recently, systematic investigations of PYP mutants under various solution conditions demonstrated that an intermediate wavelength form exists even for WT PYP in the presence of chaotropes such as thiocyanate (*16*, *20*). There are two possible origins for the intermediate wavelength form. (i) Similar to the case of the acidic form, the phenolic O1 of the chromophore is protonated, but chromophore−protein interactions provide a red-shift of the absorption maximum. (ii) The chromophore is deprotonated like a neutral form, but chromophore−protein interactions blue-shift the absorption maximum. For instance, recent studies using various mutant proteins (*16*, *20*) suggested that the hydrogen bond between Glu46 and phenolate O1 differs between the neutral and the intermediate wavelength forms. This idea was based on a previous FT-Raman study (*20*), which showed that the 393 nm form of the Y42F mutant exhibits a main Raman band at ∼1572 $cm^{-1}$. Because this frequency is significantly downshifted from a main Raman band (1580−1600 $cm^{-1}$) for the acidic form, it was suggested that the chromophore is not fully protonated. We should note, however, that the FT Raman experiment was performed under nonresonance conditions using a 1064 nm light. Thus, both the 393 and the 458 nm forms contributed to the spectrum, which complicates the interpretation of the data.

To determine the origin, the protonation state of the chromophore is key information. Resonance Raman spectroscopy is ideally suited for this purpose because several Raman bands are sensitive to the protonation state of the chromophore (*6*, *7*, *17*, *18*, *21*, *22*). Furthermore, resonance Raman technique has an advantage over the FT Raman method in its selectivity (i.e., a vibrational spectrum of a specific component can be selectively enhanced by tuning the laser wavelength). The resonance enhancement will allow us to measure the Raman spectrum of the intermediate wavelength forms without interference from the neutral form. To elucidate the structure of the intermediate wavelength form, we apply resonance Raman spectroscopy to WT PYP and some mutants (Tyr42 → Ala; Y42A, Tyr42 → Phe; Y42F, Glu46 → Gln; E46Q, Thr50 → Val; T50V) in the presence or absence of potassium thiocyanate. Quantum chemical calculations based on density functional theory (DFT) are performed to examine the effects of hydrogen bonding as well as a dielectric constant near the active site on the chromophore protonation.

[2] The acidic form was denoted as $PYP_{M,dark}$ in our previous publications (*7*, *17*, *18*).

## MATERIALS AND METHODS

*Sample Preparation.* Production of WT PYP and Y42A, Y42F, E46Q, and T50V mutants apoprotein by *Escherichia coli*, reconstitution of the holoprotein with the chromophore, and the subsequent protein purification were performed as described previously (*10*, *23*). PYP in buffered $D_2O$ (90% $D_2O$/10% $H_2O$) was prepared by proper dilution of a concentrated protein in 100 mM Tris/HCl buffer at pH 7.4 into $D_2O$, and then the sample was incubated overnight at room temperature before the measurements were taken. The $^{13}C$-labeled 4-hydroxycinnamic acid was synthesized as described previously (*18*). $^{13}C$-labeled PYP was prepared by reconstitution of apoprotein with 4-hydroxycinnamic anhydride whose ring carbon atoms (C1−C6) were labeled with $^{13}C$.

*Resonance Raman Spectroscopy.* Resonance Raman spectra were obtained as described earlier (*7*, *17*, *18*). A liquid nitrogen cooled CCD detector (Instrument S. A., Inc.) recorded the Raman spectra after a Triax190 spectrometer (Instrument S. A., Inc.) removed the excitation light, and a Spex 500M spectrometer (1800 or 3600 grooves/mm grating, 0.5 m focal length) dispersed the scattered light. The 406.7 nm line from a krypton ion laser (BeamLok 2065, Spectra-Physics Lasers, Inc.) or the 325.0 nm line from a helium−cadmium laser (IK5651R-G, Kimmon Electric Co., Ltd.) excited the samples at a 90° angle relative to the axis of the collection optics. A polarization scrambler is placed at the entrance of the spectrometer. All spectra were taken at room temperature (∼23 °C), and homemade software eliminated the noise spikes in the spectra caused by cosmic rays. All Raman spectra were calibrated by using neat fenchone. Some of the spectra were baseline corrected. The measurements were made on samples contained in a quartz spinning cell (10 mm in diameter), and a rotation speed of 800 rpm was used.

*Theoretical Estimation of a $pK_a$ Value of the Chromophore.* The acid-dissociation process for given acid HA may be written as

$$AH \overset{K_a}{\rightleftharpoons} A^- + H^- \quad (1)$$

Then the acid-dissociation constant $K_a$ is related to the standard thermodynamic relationship

$$-RT \ln K_a = \Delta G = G(H^+) + G(A^-) - G(HA) \quad (2)$$

At temperature $T$, the $pK_a$ is given by

$$pK_a = \{G(H^+) + G(A^-) - G(HA)\}/2.303RT \quad (3)$$

In this study, we consider the following equilibrium in the active site of PYP:

$$AH + B^- \rightleftharpoons A^- + BH \quad (4)$$

where AH, $B^-$, $A^-$, and BH are protonated Glu46, deprotonated chromophore, deprotonated Glu46, and protonated

Table 1: Absorption Maxima (nm) of Wild-Type PYP and Mutants under Various Conditions

| | pH 11[a] | pH 7.4[b] | pH 4.0[c] | pH 2.0[d] | 4 M KSCN[e] |
|---|---|---|---|---|---|
| WT | | 446 | | 349 | 365 |
| Y42A | 440 | 374 | 355 | 351[f] | |
| Y42F | | 458/393[g] | 359 | 350[h] | |
| E46Q | | 460 | | 348 | 359 |
| T50V | | 457 | | 348 | 362 |

[a] 10 mM Tris-NaOH, pH 11. [b] 10 mM Tris-HCl, pH 7.4. [c] 10 mM Tris-HCl, pH 4.0. [d] 20 mM citrate/HCl, pH 2.0. [e] 10 mM Tris-HCl, 4 M KSCN, pH 7.4. [f] 10 mM Tris-HCl, pH 2.5. [g] The 393 nm peak was observed as a shoulder of a main absorption band at 458 nm. [h] 10 mM Tris-HCl, pH 2.7.

chromophore, respectively. Then the relative p$K_a$ of BH to AH is calculated by (*24*, *25*)

$$\begin{aligned}\Delta \mathrm{p}K_a &= \{G(\mathrm{AH} + \mathrm{B}^-) - G(\mathrm{A}^- + \mathrm{BH})\} \\ &= \Delta G/2.303RT \\ &= (\Delta E + \Delta \mathrm{p}V + T\Delta S)/2.303RT \end{aligned} \quad (5)$$

As the $\Delta pV$ and $T\Delta S$ terms are very small as compared to the energy difference $\Delta E$ (*26*), they can be neglected, and

$$\Delta \mathrm{p}K_a \approx \Delta E/2.303RT \quad (6)$$

where $\Delta E$ is obtained as the energy difference in each state from DFT calculations.

*DFT Calculations.* The gas-phase geometries and electronic energies were calculated using the DFT method via the Gaussian98 program (*27*). The hybrid functional B3LYP and the 6-31G** basis set were used for these calculations. The geometry optimizations were performed in the gas phase without constraints except for a protonated chromophore where the O1−H distance was fixed at 0.967 Å. Once we obtained an optimized geometry, we computed the energy using the Onsager reaction field method (*28*) to take into account the dielectric constant in the protein.

## RESULTS

*UV−Vis Absorption Spectra.* Figure 2A−C shows the dramatic pH-dependence of the absorption spectra of Y42A PYP, which are consistent with those presented by Imamoto et al. (*10*). The absorption maximum at different pH values was calculated from a first derivative of the spectra, and the estimated values are summarized in Table 1. As shown in Figure 2A, the absorption maximum at pH 11 is 440 nm with a clear shoulder at 374 nm. Lowering the pH makes the 374 nm band as a main absorption band with a shoulder at 440 nm (Figure 2B). At pH 4.0, the 374 nm form is converted to a new species whose absorption maximum is 355 nm (Figure 2C). Further lowering the pH shifts the absorption maximum from 355 to ~350 nm. Y42F PYP shows an absorption maximum at 458 nm and a shoulder at 393 nm (not shown). These absorption maxima continuously shift to 350 nm upon lowering the pH from 7.4 to 2.7. Although an intermediate wavelength form is not detected for WT PYP and the E46Q and T50V mutants (*10*), the absorption maximum at pH <2.5 was ~350 nm (Figure 2D; Table 1). In Figure 2E,F, we also examine the effect of KSCN on the absorption spectra of WT PYP and the E46Q and T50V mutants. As can be seen in the figure, the addition

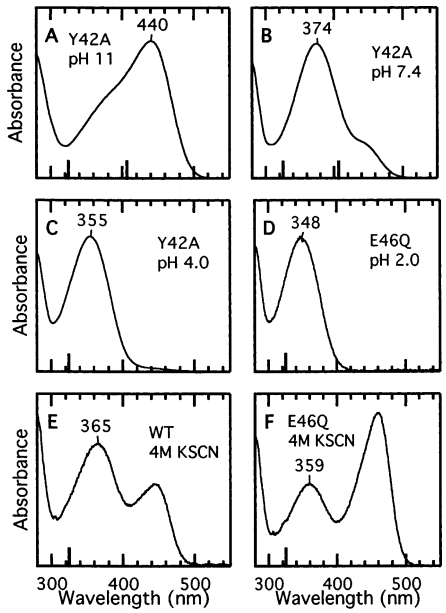


FIGURE 2: Optical absorption spectra of wild-type PYP and mutants. The vertical lines indicate the excitation wavelengths at which resonance Raman spectra were collected.

of 4 M KSCN produces a species whose absorption maximum is 359−365 nm. The observed absorption spectrum for WT PYP (Figure 2E) agrees well with that reported previously (*16*). We should note, however, that Glu46 mutants including E46Q have been reported to exhibit no intermediate wavelength form in the presence KSCN (*16*). This result contradicts the present observation that the absorption spectrum of E46Q PYP with 4 M KSCN contains a band at 359 nm (Figure 2F). Because the contribution of the 359 nm species for E46Q PYP is significantly weak as compared with those of WT and T50V, small differences in experimental conditions such as buffer compositions may prevent its formation in their case.

*Resonance Raman Spectra of an Intermediate Wavelength Form.* Figures 3 and 4 display the resonance Raman spectra of WT PYP and the Y42A, Y42F, E46Q, and T50V mutants at various pH values, respectively. These spectra are obtained with the 325.0 nm excitation, which is in resonance with the absorption band for the 345−393 nm species, while it is out of resonance with the absorption band for the 440−460 nm species.

*(A) Wild-Type PYP.* The resonance Raman spectra of WT PYP above pH 4.0 (Figure 3, traces a−c) exhibit an intense doublet near 1577/1596 $cm^{-1}$ as well as several bands with moderate intensities at 1440, 1289, and 1173 $cm^{-1}$. These spectra are distinctly different from the 406.7 or 413.1 nm excitation spectrum of WT PYP at pH 7.4 (*6*, *7*, *17*), indicating the presence of a minor species that absorbs light at 325 nm. Note that the observed spectrum is distinctly different from that of $PYP_M$, which can be also observed at the 325.0 nm excitation (*7*, *18*). For instance, the spectral features around 1300 and 700−900 $cm^{-1}$ are different. The resonance Raman spectrum at pH 2.0 (Figure 3, trace e) is consistent with that reported previously (*17*, *18*), and it can be ascribed to an acidic form of WT PYP. The spectrum at pH 3.0 (Figure 3, trace d) is similar to that obtained at pH 2.0. The doub1et around 1580/1600 $cm^{-1}$ is assigned to coupled C−C and C═C stretching modes $\nu_{14}/\nu_{13}$ of the

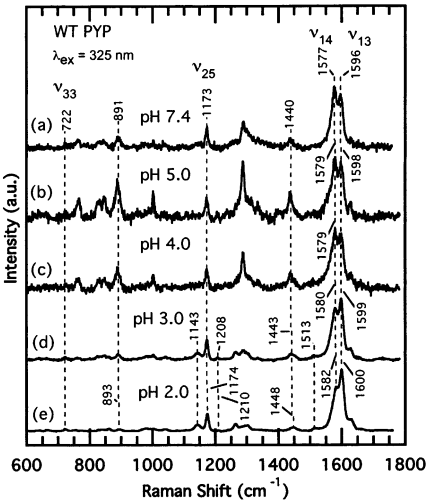


FIGURE 3: Resonance Raman spectra of wild-type PYP. The spectra were obtained at 325.0 nm excitation. The protein concentration was 100 $\mu$M in all the experiments. The following list gives the buffer condition: (a) 10 mM Tris/HCl at pH 7.4; (b) 10 mM citrate/20 mM phosphate buffer at pH 5.0; (c) 10 mM citrate/20 mM phosphate buffer at pH 4.0; (d) 10 mM citrate/20 mM phosphate buffer at pH 3.0; and (e) 20 mM citrate/HCl buffer at pH 2.0.

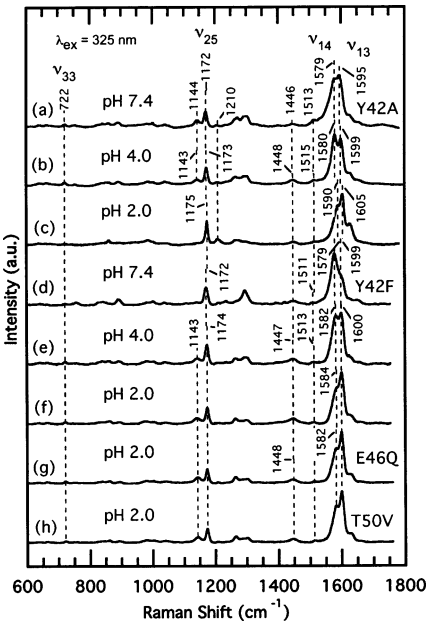


FIGURE 4: Resonance Raman spectra of Y42A, Y42F, E46Q, and T50V mutants of PYP. The spectra were obtained at 325.0 nm excitation. The following list gives the sample, protein concentration, and buffer condition: (a) Y42A, 100 $\mu$M, 10 mM Tris/HCl at pH 7.4; (b) Y42A, 100 $\mu$M, 10 mM citrate/20 mM phosphate buffer at pH 4.0; (c) Y42A, 50 $\mu$M, 20 mM citrate/HCl buffer at pH 2.0; (d) Y42F, 100 $\mu$M, 10 mM Tris/HCl at pH 7.4; (e) Y42F, 100 $\mu$M, 10 mM citrate/20 mM phosphate buffer at pH 4.0; (f) Y42F, 50 $\mu$M, 20 mM citrate/HCl buffer at pH 2.0; (g) E46Q, 100 $\mu$M, 20 mM citrate/HCl buffer at pH 2.0; and (h) T50V, 100 $\mu$M, 20 mM citrate/HCl buffer at pH 2.0.

aromatic ring and vinyl group of the chromophore, respectively (*17*, *18*). These Raman bands are important because their frequency is highly sensitive to the protonation state of the chromophore (*6*, *7*, *17*). Lowering the pH slightly upshifts the doublet, and the spectrum at pH 2.0 shows the bands at 1582/1600 cm$^{-1}$. The intensity ratio of the doublet also changes by decreasing the pH (i.e., the higher frequency $\nu_{13}$ band becomes larger at lower pH). In Figure 5A, the

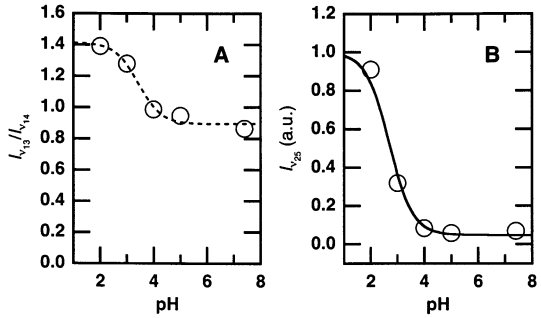


FIGURE 5: (A) The effect of pH on the peak intensity of $\nu_{13}$ relative to that of $\nu_{14}$ for wild-type PYP. The dotted line represents the fitted curve with p$K_a$ = 3.4 ± 0.4. (B) pH dependence of the integrated peak intensity of $\nu_{25}$ for wild-type PYP. The solid line represents the fitted curve with p$K_a$ = 2.7 ± 0.2. The peak intensity is normalized to be 0.9 at pH 2.0 (see text for details). Experimental conditions are the same as those given in Figure 3.

intensity of the $\nu_{13}$ band relative to that of $\nu_{14}$ is plotted as a function of pH. The relative intensity as well as overall spectral features gradually changes even above pH 4.0 (Figures 3 and 5A). This result indicates that the observed pH-dependence does not follow a simple two-state model, although an application of a simple Henderson−Hasselbalch equation (*29*) to the data (dotted line in Figure 5A) provides a p$K_a$ value of 3.4 ± 0.4. Another Raman band that is sensitive to the protonation state of the chromophore is a C−H bending mode of the chromophore aromatic ring $\nu_{25}$ (*7*, *18*), which is assigned to a band near 1173 cm$^{-1}$. The frequency of $\nu_{25}$ is only slightly affected by the pH. In Figure 5B, the integrated intensities of the sharp $\nu_{25}$ band are plotted by changing pH. The data are fitted to Henderson−Hasselbalch equation with an assumption that the $\nu_{25}$ intensity at pH 2.0 is 0.9. This assumption implies that the fraction of the acidic form is 90% at pH 2.0 (*10*, *20*) and gives rise to a p$K_a$ of 2.7 ± 0.2. This agrees well with the p$K_a$ of 2.8 for protonation of the chromophore in WT PYP (*10*, *16*).

*(B) Tyr42Ala and Tyr42Phe Mutants.* Figure 4 examines the effects of pH on the resonance Raman spectra of Y42A (Figure 4, traces a−c) and Y42F mutants (Figure 4, traces d−f). Because Y42A PYP mainly contains the 374, 355, and 350 nm species at pH 7.4, 4.0, and 2.0, respectively (Figure 2), the observed spectra can be ascribed to the corresponding species. The resonance Raman spectra of the Y42A mutant contain an intense doublet around 1580/1600 cm$^{-1}$ and some bands near 1448, 1300, and 1172 cm$^{-1}$. These spectral features resemble those for WT PYP (Figure 3). Furthermore, lowering the pH leads to small upshifts of the $\nu_{14}/\nu_{13}$ doublet as well as changes in the intensity ratio. At pH 7.4, the 374 nm species exhibits the doublet at 1579/1595 cm$^{-1}$, whereas the corresponding Raman band is observed at 1590/1605 cm$^{-1}$ for the 350 nm species at pH 2.0. The higher frequency $\nu_{13}$ band becomes larger at pH 2.0. Traces d−f in Figure 4 are the resonance Raman spectra of the 393−350 nm species of Y42F PYP. The spectra have an intense doublet around 1580/1600 cm$^{-1}$ and some bands near 1448, 1300, and 1172 cm$^{-1}$. These Raman bands exhibit a similar intensity and frequency pattern to those of WT PYP and the Y42A mutant. In addition, similar to the case of WT and the Y42A mutant, the $\nu_{14}/\nu_{13}$ doublet slightly upshifts and changes in its intensity ratio upon lowering pH. In Figure 4, we also present the resonance Raman spectra of the acidic form ($\lambda_{max}$ = 348 nm) of the E46Q and T50V mutants at pH 2.0 (Figure 4,

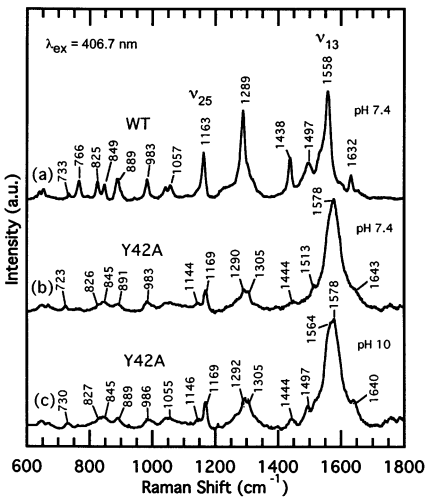


FIGURE 6: Resonance Raman spectra of wild-type PYP and Y42A mutant. The spectra were obtained at 406.7 nm excitation. The following list gives the sample, protein concentration, and buffer condition: (a) wild-type, 76 $\mu$M, 10 mM Tris/ HCl buffer at pH 7.4; (b) Y42A, 70 $\mu$M, 10 mM Tris/HCl buffer at pH 7.4; and (c) Y42A, 140 $\mu$M, 50 mM bicarbonate/100 mM hydroxide buffer at pH 10.0.

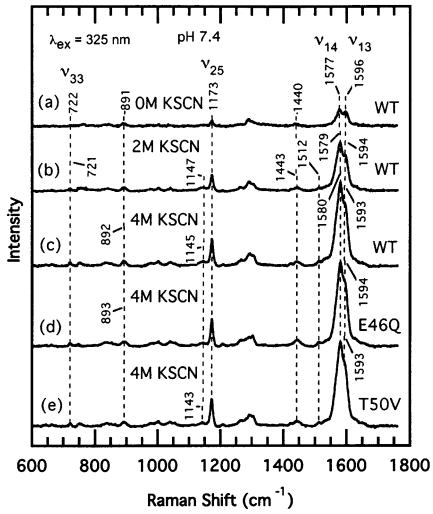


FIGURE 7: Effect of potassium thiocyanate on the resonance Raman spectra of wild-type PYP and mutants in 10 mM Tris/HCl buffer at pH 7.4: (a) wild-type; (b) wild-type, 2 M KSCN; (c) wild-type, 4 M KSCN; (d) E46Q, 4 M KSCN; and (e) T50V, 4 M KSCN. The spectra were obtained at 325.0 nm excitation.

traces g and h). These spectra are almost the same as that of WT PYP (trace e in Figure 3).

Figure 6 shows the resonance Raman spectra of WT PYP and the Y42A mutant at 406.7 nm excitation. The spectrum of WT PYP (Figure 6, trace a) is consistent with the previous works (*6*, *7*, *17*), although it differs considerably from the 325.0 nm excitation spectrum (Figure 3, trace a). Similarly, Y42A PYP at pH 7.4 exhibits clear dependence on the excitation wavelength. The excitation wavelength of 406.7 nm is on resonance with the absorption band for both the 374 and the 440 nm species of Y42A PYP. The presence of these species explains the 406.7 nm excitation spectra of Y42A PYP (i.e., the 440 nm species has an intense $\nu_{13}$ band at ~1560 cm$^{-1}$ like WT PYP, whereas the 374 nm species contains an intense $\nu_{14}/\nu_{13}$ doublet at 1579/1593 cm$^{-1}$). The contribution from these species makes a broad Raman band centered at 1577 cm$^{-1}$. Analogously, the observed 1169 cm$^{-1}$ band is interpreted as a superposition of two $\nu_{25}$ bands at 1172 and ~1165 cm$^{-1}$ for the 374 and 440 nm forms, respectively. The resonance Raman spectrum of Y42A PYP at pH 10 supports that the 440 nm species exhibits the ~1560 cm$^{-1}$ band: the shoulder at ~1560 cm$^{-1}$ increases in intensity as the fraction of the 440 nm species is increased by changing pH from 7.4 to 10 (Figure 6, trace b → c). These results imply that the 440 nm form of Y42A PYP is characterized by a $\nu_{25}$ band at ~1165 cm$^{-1}$ and an intense $\nu_{13}$ band at ~1560 cm$^{-1}$.

*Effect of KSCN on Wild-Type and Glu46Gln and Thr50Val Mutants.* The upper three traces of Figure 7 show the resonance Raman spectra of WT PYP at pH 7.4 in the presence or absence of KSCN. Addition of a high concentration of KSCN increases Raman intensities. Although both the 446 and the 365 nm species are present even at the highest 4 M KSCN (Figure 2E), the excitation light at 325.0 nm selectively measures the resonance Raman spectrum of the 365 nm form of WT PYP. The main spectral features for the 365 nm form (Figure 7, trace c) are similar to those for the acidic 350 nm form (Figure 3, trace e). These spectra

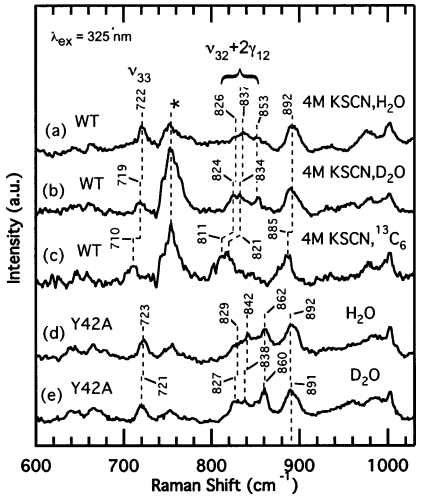


FIGURE 8: Resonance Raman spectra of wild-type PYP and Y42A mutant in 10 mM Tris/HCl buffer, pH or pD 7.4: (a) wild-type, 100% $H_2O$, 4 M KSCN; (b) wild-type, 90% $D_2O$/10% $H_2O$, 4 M KSCN; (c) $^{13}C_6$-ring PYP, 4 M KSCN; (d) Y42A, 100% $H_2O$; and (e) Y42A, 90% $D_2O$/10% $H_2O$. The spectra were obtained with 325.0 nm excitation. The feature with the asterisk is due to an imperfect subtraction of the KSCN Raman band.

are characterized by an intense doublet near 1580/1600 cm$^{-1}$ with some bands around 1440, 1300, and 1173 cm$^{-1}$, although the frequencies as well as the intensities are somewhat different. In Figure 7, we also demonstrate the resonance Raman spectra of the E46Q and T50V mutants in the presence of 4 M KSCN (Figure 7, traces d and e). As can be seen, these spectra for the mutants are very similar to that of WT PYP.

*Effects of $D_2O$ on the Resonance Raman Spectra.* We previously showed that the deuteration effects on the $\nu_{32} + 2\gamma_{12}$ doublet around 850 cm$^{-1}$ and the $\nu_{33}$ band around 720 cm$^{-1}$ act as a marker for the protonation state of the chromophore (*18*). These Raman bands are examined in Figure 8, which displays the 600−1000 cm$^{-1}$ region of the resonance Raman spectra of the 365 nm form of WT PYP in the presence of 4 M KSCN and the spectra of the 374 nm form of the Y42A mutant. For WT PYP, Figure 8 presents

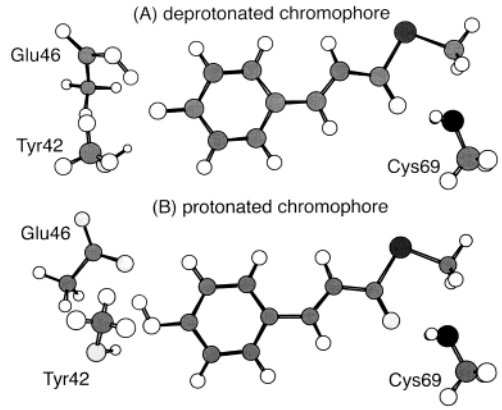


FIGURE 9: Optimized structures of the active site model of PYP.

the spectra of the 365 nm form in buffered $H_2O$ and $D_2O$ solutions as well as PYP whose chromophore is labeled with $^{13}C$ at the ring carbon atoms ($^{13}C_6$-ring). Either H/D or $^{12}C/^{13}C$ isotopic substitution causes some changes around 720 and 830−860 cm$^{-1}$. The $\nu_{33}$ mode includes O1−C1 and C4−C7 stretching coordinates such as Y13 of tyrosine (*18*, *30*). This mode is observed at 721 cm$^{-1}$ for the protonated chromophore in $PYP_M$ and exhibits 3 and 9 cm$^{-1}$ downshifts upon deuterium substitution of the hydroxyl group and $^{13}C_6$-ring labeling, respectively (*18*). We assign the 721 cm$^{-1}$ band to $\nu_{33}$ on the basis of its −2 cm$^{-1}$ $D_2O$ and −10 cm$^{-1}$ $^{13}C_6$-ring shifts. The ring-breathing vibration $\nu_{32}$ is observed as a broad Raman band at ∼850 cm$^{-1}$ for WT $PYP_M$ (*18*). This band arises from the Fermi resonance of $\nu_{32}$ with the overtone of an out-of-plane ring-bending vibration $\gamma_{12}$. Because of the removal of the Fermi resonance upon deuteration of the phenolic OH group, the band shape of the doublet significantly changes in $D_2O$ solutions. In addition, this band is expected to show a large downshift (∼20 cm$^{-1}$) upon $^{13}C_6$-ring substitution (*18*). Thus, the H/D and $^{12}C/^{13}C$-sensitive features around 830−860 cm$^{-1}$ in traces a−c of Figure 8 are assigned at least in part to the $\nu_{32} + 2\gamma_{12}$ doublet. Traces d and e of Figure 8 are the resonance Raman spectra of the 374 nm form of Y42A PYP in buffered $H_2O$ and $D_2O$ solutions, respectively. Similar to the case of the 365 nm form in WT PYP, the $D_2O$-sensitive features at 722 and 830−840 cm$^{-1}$ can be assigned to $\nu_{33}$ and $\nu_{32} + 2\gamma_{12}$, respectively.

On the basis of these experimental observations, we will discuss the protonation state of the chromophore in the Discussion.

*DFT Calculations—Estimation of p$K_a$.* To examine how a protein moiety controls the protonation state of the chromophore, we have carried out DFT calculations and estimated a p$K_a$ value of the chromophore. For these calculations, 4-hydroxycinnamyl methyl thiolester (HCMT) is employed as a chromophore model. We used *trans*-HCMT and placed methanol, acetic acid, and methylamine as a model for Tyr42, Glu46, and the backbone amide of Cys69, respectively. These components were arranged on the basis of the crystal structure of WT PYP (*5*) and subsequently optimized to yield the structures illustrated in Figure 9. In Figure 9A, the phenolic O1 of HCMT is deprotonated, whereas the carboxylic group of acetic acid (Glu46) is protonated. In Figure 9B, HCMT and acetic acid are protonated and deprotonated, respectively. These structures were used for the calculation of $\Delta pK_a$ between chromophore and Glu46 by eq 6. We also performed DFT calculations of other models having no Tyr42 (methanol) or Cys69 (methylamine) to examine the effect of hydrogen bonds with these residues. For each case, the optimized structure was used for the calculations of $\Delta pK_a$. In addition, to consider the effect of the protein environment, electronic energies were calculated by taking into account the dielectric constant in protein. We employed the Onsager reaction field method (*28*), which places a model molecular system in a spherical cavity with a radius $a_0$, surrounded by a continuous medium of a dielectric constant $\epsilon$. In this study, $\epsilon$ was varied from 2.0 to 80, and the radius $a_0$ was determined from the volume of the model molecular system. Table 2 gives the computed $\Delta E$ and $\Delta pK_a$ for the three models. It is clear that interactions between chromophore and protein significantly affect $\Delta pK_a$.

Table 2: Calculated Energy Difference (kJ mol$^{-1}$) and $\Delta pK_a$ between the Phenolic O1 of the Chromophore and the Carboxylic Group of Glu46

| | chr. + E46, Y42, C69 (WT) | | chr. + E46, C69 (Y42A or Y42F) | | chr. + E46, Y42 | |
|---|---|---|---|---|---|---|
| $\epsilon$[a] | $\Delta E$[b] | $\Delta pK_a$ | $\Delta E$[b] | $\Delta pK_a$ | $\Delta E$[b] | $\Delta pK_a$ |
| 1 | −52.93 | −9.3 | −36.29 | −6.4 | −51.94 | −9.1 |
| 2 | −37.92 | −6.6 | −16.39 | −2.9 | −40.67 | −7.1 |
| 4 | −25.19 | −4.4 | 1.29 | −0.2 | −31.21 | −5.5 |
| 10 | −14.20 | −2.5 | 17.04 | 3.0 | −23.17 | −4.1 |
| 20 | −9.86 | −1.7 | 23.64 | 4.1 | −19.92 | −3.5 |
| 40 | −7.45 | −1.3 | 27.27 | 4.8 | −18.15 | −3.2 |
| 80 | −6.20 | −1.1 | 29.18 | 5.1 | −17.23 | −3.0 |

[a] Dielectric constant. [b] Based on B3LYP/6-31G** electronic energies. $\Delta E$ = $E$(deprotonated HCMT + protonated Glu46) − $E$(protonated HCMT + deprotonated Glu46).

## DISCUSSION

*Structure of Intermediate Wavelength Forms.* Previous Raman studies on PYP and a chromophore model (*6*, *7*, *17*, *18*) have shown that the $\nu_{25}$ and $\nu_{14}/\nu_{13}$ modes of the protonated *trans*- or *cis*-chromophore are at ∼1174 and ∼1580/1600 cm$^{-1}$, respectively, whereas the deprotonated *trans*-chromophore exhibits the $\nu_{25}$ band at ∼1163 cm$^{-1}$ and a single band of $\nu_{13}$ at ∼1560 cm$^{-1}$. In this study, we have shown that the resonance Raman spectra for the intermediate wavelength forms are very similar to those of the acidic forms. For example, the 374−393 nm forms of the Y42A and Y42F mutants exhibit the $\nu_{14}/\nu_{13}$ doublet around 1579/1595 cm$^{-1}$ and $\nu_{25}$ band at 1172 cm$^{-1}$ (Figure 4). Analogously, the resonance Raman spectra of the 360−365 nm form of WT PYP and E46Q and T50V mutants in the presence of 4 M KSCN are characterized by the $\nu_{14}/\nu_{13}$ doublet at 1580/1593 cm$^{-1}$ and the $\nu_{25}$ band at 1173 cm$^{-1}$ (Figure 7). These results indicate that the chromophore of the intermediate wavelength form is protonated. We should note that the 325.0 nm excitation spectrum of WT PYP above pH 4.0 resembles that of the Y42A or Y42F mutant (Figures 3 and 4). This observation implies that WT PYP contains a minor component whose chromophore is protonated even at neutral pH. Thus, an intermediate wavelength form is in equilibrium with a main neutral form at pH 7.4, and either addition of KSCN or Tyr42 mutation increases a fraction of this form. If we assume that the intensity of the $\nu_{25}$ band at 1173 cm$^{-1}$ remains the same in the examined pH region, Figure 5B indicates that the fraction of the intermediate

wavelength form is estimated to be about 5% in WT PYP above pH 4. Further evidence for the protonation state of the chromophore is obtained from deuterium isotope effects on the spectrum. We recently demonstrated that the deuteration effect on the $\nu_{32} + 2\gamma_{12}$ doublet around 850 $cm^{-1}$ acts as a marker for the protonation state of the chromophore (*18*). This is identical to the case of the tyrosine doublet, where the intensity ratio of the doublet is a measure of the protonation or the state of hydrogen bonding of the phenolic OH group (*30*). The $\nu_{33}$ band for the protonated chromophore (ca. 720 $cm^{-1}$) is also sensitive to H/D substitution since this mode includes the O1−C1 stretching coordinate like Y13 of tyrosine (*18, 30*). As shown in Figure 8, both $\nu_{33}$ and $\nu_{32} + 2\gamma_{12}$ are $D_2O$ sensitive, providing further evidence for the protonated chromophore of the intermediate wavelength form of PYP.

Here, we comment on a previous FT-Raman investigation of Y42F PYP, which suggested that the chromophore of the 393 nm form is not fully protonated (*20*). The previous study showed that a main Raman band for the 393 nm form is observed at ∼1572 $cm^{-1}$ as a shoulder of a large Raman band at 1552 $cm^{-1}$ for the 458 nm form. In contrast, the resonance Raman spectrum of the 393 nm form at pH 7.4 has the $\nu_{14}/\nu_{13}$ doublet at 1579/1599 $cm^{-1}$, although the peak intensity of the $\nu_{13}$ band is significantly smaller than that of the $\nu_{14}$ band (Figure 4). This result clearly indicates that the chromophore of the 393 nm form is protonated. The presence of the $\nu_{13}$ band at 1599 $cm^{-1}$ was not clear in the reported FT-Raman spectrum because of its small intensity as well as a strong overlap with a large 1552 $cm^{-1}$ band of the 458 nm form.

Recent acid/base titration experiments of WT PYP and mutants suggested that the acidic species is formed by protonation of the phenolic O1 as a secondary result of acid denaturation of the protein moiety (*16*). The denatured protein implies an absence of specific chromophore−protein interactions in the acidic form. This idea is consistent with the present finding that the resonance Raman and absorption spectra of the acidic form are little affected by the amino acid replacements (Figures 2−4). In contrast, spectral properties of the intermediate wavelength form depend on mutations. For instance, there are some distinct differences in the resonance Raman spectra of the intermediate wavelength form between WT PYP and Y42A mutant (Figures 3 and 4), indicating that the protein moiety is not denatured. On the other hand, thiocyanate is known as a chaotropic salt, which destabilizes and denatures proteins by increasing the solvation of the polar peptide backbone (*31*). Thus, the protein moiety in the presence of KSCN will be partially unfolded. We therefore suggest that the addition of KSCN causes protein partial unfolding, which changes the resonance Raman spectrum of the chromophore through altered chromophore−protein interactions.

As can be seen in Figures 3, 4, and 7, the resonance Raman spectra of the protonated chromophore exhibit a similar intensity and frequency pattern (i.e., an intense doublet at 1580/1600 $cm^{-1}$ and some bands were observed around 1445, 1300, and 1173 $cm^{-1}$). There are, however, some distinct differences in the spectra. One of the characteristic differences is the presence or absence of a band at ∼1143 $cm^{-1}$. This Raman band is present for the acidic forms of WT PYP and the Y42F, E46Q, and T50V mutants. In addition, the 374 nm form of Y42A PYP as well as the intermediate wavelength form in the presence of KSCN exhibit a similar band. We recently measured the resonance Raman spectra of the acidic form of WT PYP and found that the band at 1143 $cm^{-1}$ is sensitive to the $^{12}C/^{13}C$ substitution of the carbonyl carbon atom.[3] Normal coordinate calculations based on DFT suggest that the presence or absence of this band correlates with the conformation around the C−C single bond of the −C═C−C(═O)−S− fragment of the chromophore. Further studies for this point are currently in progress.

*Mechanism of Spectral Tuning in PYP. (A) Hydrogen Bonding at the Phenolic O1.* As discussed previously, the present resonance Raman study demonstrates that the chromophore of the intermediate wavelength form is protonated. This finding indicates that protonation of the chromophore is responsible for a blue-shift in the absorption maximum from 446 to 355−393 nm. Such a large shift (5700−3000 $cm^{-1}$) is consistent with a previous study of Kroon et al. (*32*) who estimated the contribution of the chromophore protonation to be around 4700 $cm^{-1}$. The p$K_a$ for protonation of the chromophore in WT PYP is ∼3 (*1*). Thus, in the case of Y42A PYP, the replacement of Tyr42 with Ala raises the p$K_a$ from 3 to 10 (*10*), and a large fraction of the chromophore is protonated at neutral pH. The present DFT calculations support the idea that the chromophore−protein hydrogen bond is important for controlling the protonation state of the chromophore. As summarized in Table 2, the removal of the hydrogen bond between phenolic O1 and Tyr42 increases the $\Delta$p$K_a$ by 3−6 pH units. This implies that a disruption of the hydrogen bond destabilizes the deprotonated chromophore. The importance of a hydrogen bond at the phenolic O1 has been also suggested by a theoretical study on the basis of classical electrostatics (*33*) as well as a spectroscopic study on Glu46 → Asp or the Ala mutant PYP (*34*).

Another noteworthy result of the DFT calculations is a minor effect of the hydrogen bond at the carbonyl O2. For instance, Table 2 shows little $\Delta$p$K_a$ change (−9.3 → −9.1) upon removal of a hydrogen bond at the carbonyl O2 with $\epsilon = 1$ (gas phase), whereas a larger change (−9.3 → −6.4) is obtained for the phenolic O1. This result indicates that the hydrogen bond at the carbonyl O2 contributes little to the stabilization of the deprotonated chromophore in PYP.

*(B) Dielectric Constant in the Vicinity of the Chromophore.* A recent study using site-directed mutagenesis pointed out that the p$K_a$ of ∼3 in WT PYP does not correspond to the p$K_a$ of the chromophore in folded protein, but it represents acidic unfolding of the protein resulting in exposure of the chromophore to solvent and an increase in its p$K_a$ (*16*). This idea suggests that the Y42A mutation not only removes a hydrogen bond between phenolic O1 and Tyr42 but also causes additional structural changes in the protein. For example, the substitution of Tyr with Ala will create a cavity near the chromophore. Formation of a cavity may allow an entry of a water molecule, which will increase an effective dielectric constant near the chromophore. This idea is consistent with DFT calculations (Table 2), which demonstrate that the surrounding dielectric constant significantly

[3] Unno, M., Kumauchi, M., Tokunaga, F., and Yamauchi, S., unpublished observations.

affects the protonation state of the chromophore. For example, in the case of the WT PYP model, an increase in $\epsilon$ from 1 (gas phase) to 80 (water) alters the $\Delta pK_a$ from −9.3 to −1.1. Recent theoretical studies on the proton transfer or $\Delta pK_a$ between Glu46 and chromophore reported a similar result for the effect of the dielectric constant near the chromophore (*35*, *36*). This indicates that higher dielectric media favor a protonated form of the chromophore. In this context, we expect that the effect of the Y42F mutation is moderate as compared to that of Y42A. In fact, the $pK_a$ for Y42F PYP is 4.4−6.4 (*10*, *16*), and the substitution of Tyr with Phe only raises the $pK_a$ by 1.5−3.5 pH units. We therefore suggest that both the dielectric constant in the vicinity of the chromophore and the hydrogen bonds at the phenolic O1 regulate the chromophore $pK_a$.

It has been established that the photocycle of PYP involves changes in the protonation state of the chromophore. For example, the $PYP_L \rightarrow PYP_M$ process involves protonation of the phenolic O1 of the chromophore (*7*). This implies that the chromophore $pK_a$ increases during the $PYP_L \rightarrow PYP_M$ transition. The results shown in this study suggest that either removal or weakening of a hydrogen bond at the phenolic O1 or increases in the dielectric constant near the chromophore is responsible for the $pK_a$ increase. In fact, recent quantum chemical calculations of the chromophore $pK_a$ in PYP suggest that a slight conformational difference in the protein structure causes a significant change in the electrostatic nature of the environment, which results in the alternation of the chromophore $pK_a$ (*36*).

In conclusion, we have performed the resonance Raman investigations of WT PYP and several mutants under various conditions and showed that the chromophore in the intermediate wavelength form is protonated. The DFT calculations are also conducted to examine how chromophore−protein interactions affect the chromophore $pK_a$. These experimental and theoretical studies suggest that both the low dielectric constant in the vicinity of the chromophore and the hydrogen bonds at the phenolic O1 are key factors that lower the chromophore $pK_a$. The resulting low $pK_a$ leads to a formation of the deprotonated chromophore at neutral pH and hence contributes to the tuning of the absorption spectrum of PYP.

## ACKNOWLEDGMENT

We are grateful to K. Yoshihara (Suntory Institute for Bioorganic Research) for assistance in preparing the $^{13}C$-labeled compound.

## REFERENCES

1. Meyer, T. E. (1985) Isolation and characterization of soluble cytochromes, ferredoxins, and other chromophoric proteins from the halophilic phototrophic bacterium *Ectothiorhodospira halophila*, *Biochim. Biophys. Acta 806*, 175−183.
2. Pellequer, J.-L., Wager-Smith, K. A., Kay, S. A., and Getzoff, E. D. (1998) Photoactive yellow protein: A structural prototype for the three-dimensional fold of the PAS domain superfamily, *Proc. Natl. Acad. Sci. U.S.A. 95*, 5884−5890.
3. Hoff, W. D., Düx, P., Hård, K., Devreese, B., Nugteren-Roodzant, I. M., Crielaard, W., Boelens, R., Kaptein, R., Van Beeumen, J., and Hellingwerf, K. J. (1994) Thiol ester-linked *p*-coumaric acid as a new photoactive prosthetic group in a protein with rhodopsin-like photochemistry, *Biochemistry 33*, 13959−13962.
4. Baca, M., Borgstahl, G. E. O., Boissinot, M., Burke, P. M., Williams, D. R., Slater, K. A., and Getzoff, E. D. (1994) Complete chemical structure of photoactive yellow protein: Novel thioester-liked 4-hydroxycinnamyl chromophore and photocycle chemistry, *Biochemistry 33*, 14369−14377.
5. Borgstahl, G. E. O., Williams, D. R., and Getzoff, E. D. (1995) 1.4 Å structure of photoactive yellow protein, a cytosolic photoreceptor: Unusual fold, active site, and chromophore, *Biochemistry 34*, 6278−6287.
6. Kim, M., Mathies, R. A., Hoff, W. D., and Hellingwerf, K. J. (1995) Resonance Raman evidence that the thioester-linked 4-hydroxycinnamyl chromophore of photoactive yellow protein is deprotonated, *Biochemistry 34*, 12669−12672.
7. Unno, M., Kumauchi, M., Sasaki, J., Tokunaga, F., and Yamauchi, S. (2002) Resonance Raman spectroscopy and quantum chemical calculations reveal structural changes in the active site of photoactive yellow protein, *Biochemistry 41*, 5668−5674.
8. Getzoff, E. D., Gutwin, K. N., and Genick, U. K. (2003) Anticipatory active-site motions and chromophore distortion prime photoreceptor PYP for light activation, *Nat. Struct. Biol. 10*, 663−668.
9. Ujj, L., Devanathan, S., Meyer, T. E., Cusanovich, M. A., Tollin, G., and Atkinson, G. H. (1998) New photocycle intermediates in the photoactive yellow protein from *Ectothiorhodospira halophila*: Picosecond transient absorption spectroscopy, *Biophys. J. 75*, 406−412.
10. Imamoto, Y., Koshimizu, H., Mihara, K., Hisatomi, O., Mizukami, T., Tsujimoto, K., Kataoka, M., and Tokunaga, F. (2001) Roles of amino acid residues near chromophore of photoactive yellow protein, *Biochemistry 40*, 4679−4685.
11. Xie, A., Kelemen, L., Hendriks, J., White, B. J., Hellingwerf, K. J., and Hoff, W. D. (2001) Formation of a new buried charge drives a large-amplitude protein quake in photoreceptor activation, *Biochemistry 40*, 1510−1517.
12. Brudler, R., Rammelsberg, R., Woo, T. T., Getzoff, E. D., and Gerwert, K. (2001) Structure of the $I_1$ early intermediate of photoactive yellow protein by FTIR spectroscopy, *Nat. Struct. Biol. 8*, 265−270.
13. Takeshita, K., Imamoto, Y., Kataoka, M., Tokunaga, F., and Terazima, M. (2002) Thermodynamic and transport properties of intermediate states of the photocyclic reaction of photoactive yellow protein, *Biochemistry 41*, 3037−3048.
14. Chen, E., Gensch, T., Gross, A. B., Hendriks, J., Hellingwerf, K. J., and Kliger, D. S. (2003) Dynamics of protein and chromophore structural changes in the photocycle of photoactive yellow protein monitored by time-resolved optical rotatory dispersion, *Biochemistry 42*, 2062−2071.
15. Sprenger, W. W., Hoff, W. D., Armitage, J. P., and Hellingwerf, K. J. (1993) The eubacterium *Ectothiorhodospira halophila* is negatively phototactic, with a wavelength dependence that fits the absorption spectrum of the photoactive yellow protein, *J. Bacteriol. 175*, 3096−3104.
16. Meyer, T. E., Devanathan, S., Woo, T., Getzoff, E. D., Tollin, G., and Cusanovich, M. A. (2003) Site-specific mutations provide new insights into the origin of pH effects and alternative spectral forms in the photoactive yellow protein from *Ectothiorhodospira halophila*, *Biochemistry 42*, 3319−3325.
17. Unno, M., Kumauchi, M., Sasaki, J., Tokunaga, F., and Yamauchi, S. (2000) Evidence for a protonated and cis configuration chromophore in the photobleached intermediate of photoactive yellow protein, *J. Am. Chem. Soc. 122*, 4233−4234.
18. Unno, M., Kumauchi, M., Sasaki, J., Tokunaga, F., and Yamauchi, S. (2003) Assignment of resonance Raman spectrum of photoactive yellow protein in its long-lived blue-shifted intermediate, *J. Phys. Chem. B 107*, 2837−2845.
19. Mihara, K., Hisatomi, O., Imamoto, Y., Kataoka, M., and Tokunaga, F. (1997) Functional expression and site-directed mutagenesis of photoactive yellow protein, *J. Biochem. 121*, 876−880.
20. Brudler, R., Meyer, T. E., Genick, U. K., Devanathan, S., Woo, T. T., Millar, D. P., Gerwert, K., Cusanovich, M. A., Tollin, G., and Getzoff, E. D. (2000) Coupling of hydrogen bonding to chromophore conformation and function in photoactive yellow protein, *Biochemistry 39*, 13478−13486.
21. Zhou, Y., Ujj, L., Meyer, T. E., Cusanovich, M. A., and Atkkinson, G. H. (2001) Photocycle dynamics and vibrational spectroscopy of the E46Q mutant of photoactive yellow protein, *J. Phys. Chem. A 105*, 5719−5726.
22. Chosrowjan, H., Taniguchi, S., Mataga, N., Unno, M., Yamauchi, S., Hamada, N., Kumauchi, M., and Tokunaga, F. (2004) Low-frequency vibrations and their role in ultrafast photoisomerization

reaction dynamics of photoactive yellow protein (PYP), *J. Phys. Chem. B*, in press.
23. Imamoto, Y., Ito, T., Kataoka, M., and Tokunaga, F. (1995) Reconstitution photoactive yellow protein the from apoprotein and *p*-coumaric acid derivatives, *FEBS Lett. 374*, 157−160.
24. Ohno, K., Kamiya, N., Asakawa, N., Inoue, Y., and Sakurai, M. (2001) Application of an integrated MOZYME + DFT method to p$K_a$ calculations for proteins, *Chem. Phys. Lett. 341*, 387−392.
25. Nakajima, S., Ohno, K., Inoue, Y., and Sakurai, M. (2003) Quantum chemical study of the p$K_a$ control mechanism for the active center in bacteriorhodopsin and its M intermediate, *J. Phys. Chem. B 107*, 2867−2874.
26. da Silva, C. O., da Silva, E. C., and Nascimento, M. A. C. (1999) Ab initio calculations of absolute p$K_a$ values in aqueous solution I. Carboxylic acids, *J. Phys. Chem. A 103*, 11194−11199.
27. Frisch, M. J., Trucks, G. W., Schlegel, H. B., Scuseria, G. E., Robb, M. A., Cheeseman, J. R., Zakrzewski, V. G., Montgomery, J. A., Jr., Stratmann, R. E., Burant, J. C., Dapprich, S., Millam, J. M., Daniels, A. D., Kudin, K. N., Strain, M. C., Farkas, O., Tomasi, J., Barone, V., Cossi, M., Cammi, R., Mennucci, B., Pomelli, C., Adamo, C., Clifford, S., Ochterski, J., Petersson, G. A., Ayala, P. Y., Cui, Q., Morokuma, K., Malick, D. K., Rabuck, A. D., Raghavachari, K., Foresman, J. B., Cioslowski, J., Ortiz, J. V., Baboul, A. G., Stefanov, B. B., Liu, G., Liashenko, A., Piskorz, P., Komaromi, I., Gomperts, R., Martin, R. L., Fox, D. J., Keith, T., Al-Laham, M. A., Peng, C. Y., Nanayakkara, A., Gonzalez, C., Challacombe, M., Gill, P. M. W., Johnson, B., Chen, W., Wong, M. W., Andres, J. L., Gonzalez, C., Head-Gordon, M., Replogle, E. S., and Pople, J. A. *Gaussian 98*, Gaussian, Inc., Pittsburgh, PA.
28. Onsager, L. (1936) Electric moments of molecules in liquids, *J. Am. Chem. Soc. 58*, 1486−1493.
29. Voet, D., and Voet, J. G. (1990) *Biochemistry*, John Wiley & Sons, New York.
30. Takeuchi, H., Watanabe, N., and Harada, I. (1988) Vibrational spectra and normal coordinate analysis of *p*-cresol and its deuterated analogues, *Spectrochim. Acta 44A*, 749−761.
31. Baldwin, R. L. (1996) How Hofmeister ion interactions affect protein stability, *Biophys. J. 71*, 2056−2063.
32. Kroon, A. R., Hoff, W. D., Fennema, H. P. M., Gijzen, J., Koomen, G.-J., Verhoeven, J. W., Crielaard, W., and Hellingwerf, K. J. (1996) Spectral tuning, fluorescence, and photoactivity in hybrids of photoactive yellow protein, reconstituted with native or modified chromophores, *J. Biol Chem. 271*, 31949−31956.
33. Demchuk, E., Genick, U. K., Woo, T. T., Getzoff, E. D., and Bashford, D. (2000) Protonation states and pH titration in the photocycle of photoactive yellow protein, *Biochemistry 39*, 1100−1113.
34. Devanathan, S., Brudler, R., Hessling, B., Woo, T. T., Gerwert, K., Getzoff, E. D., Cusanovich, M. A., and Tollin, G. (1999) Dual photoactive species in Glu46Asp and Glu46Ala mutants of photoactive yellow protein: A pH-driven color transition, *Biochemistry 38*, 13766−13772.
35. Thompson, M. J., Bashford, D., Noodleman, L., and Getzoff, E. D. (2003) Photoisomerization and proton transfer in photoactive yellow protein, *J. Am. Chem. Soc. 125*, 8186−8194.
36. Yoda, M., Inoue, Y., and Sakurai, M. (2003) Effect of protein environment on p$K_a$ shifts in the active site of photoactive yellow protein, *J. Phys. Chem. B 107*, 14569−14575.

BI035638C